Available online at www.sciencedirect.com
ScienceDirect
International Journal of Thermal Sciences 46 (2007) 580–588
International Journal of Thermal Sciences
www.elsevier.com/locate/ijts

Fabrication, modeling and testing of a thin film Au/Ti microheater

K.L. Zhang [a,*,1], S.K. Chou [a,*], S.S. Ang [b]

[a] *Department of Mechanical Engineering, National University of Singapore, Singapore 119260*
[b] *Department of Electrical Engineering, University of Arkansas, Fayetteville, AR 72701, USA*

Received 20 May 2006; received in revised form 3 August 2006; accepted 4 August 2006

Available online 11 September 2006

Abstract

A thin film gold/titanium (Au/Ti) microheater is developed for microthruster ignition, micro explosive boiling, and micro sensor applications. The microheater was fabricated onto a Pyrex bulk substrate using a micro-fabrication technology. A finite-element based electro-thermal modeling was employed to predict the microheater performance. The variations of the microheater temperature with time, space, and power supply are determined from the modeling. A method is presented to determine the thin film Au/Ti electrical resistivity and thermal conductivity. It was found that significant differences exist between heat transfer in microheater and conventional heater. Experimental testing of the microheater temperature was performed using a customized circuitry. The finite-element model is validated by the experimental measurements.

Keywords: Microheater; Thin film; Au/Ti; Modeling; Experiment

1. Introduction

Microheaters have been widely investigated because of their extensive applications in micro gas sensors, pressure sensors, flow rate sensors, micro explosive boiling, and micro ignition of micropropulsion systems [1–10]. Solid state sensors based on semi-conducting sensing materials provide interesting solutions for various applications, ranging from health care and safety to quality control in industrial processes [1–5]. Devices based on micro explosive boiling have applications in thermal bubble jet printers, biology, medicine, space exploration, and microelectronic cooling [6,7]. A micropropulsion system is indispensable in microspacecraft for attitude control, delta-v maneuvers, station keeping, and orbit adjust [8–10]. The wire heater and thin film heater are two main kinds of microheaters. A MEMS-based thin film heater has more interesting applications than a wire heater due to its lower heat mass, ease of integration and compatibility with other MEMS-based devices.

The general requirements for a thin film microheater are low power consumption, fast response, good heat confinement, good mechanical stability, and good fabrication yield. Heavily p-doped silicon was initially used for the microheater material because of its excellent mechanical properties [2]. Nevertheless, this kind of microheater shows some limitations due to its relatively high power consumption. To improve the microheater performance, many recent studies employ dielectric membranes to assure lower power consumption [3–5,8]. Dielectric membranes do provide improvement in terms of microheater power consumption. However, they could be less reliable for some applications in harsh environments. For thin film microheater, modeling is a good way to predict its performance, especially its detailed temperature profile [2,4,5,8]. Unfortunately, the thin film material properties are seldom discussed in detail, which are essential to the microheater performance prediction. The temperature variations of thin film material electrical resistivity and thermal conductivity are often ignored. It should be noted that these are the key material properties required for any thin film microheater modeling. Furthermore, some important modeling techniques and experimental procedures such as meshing strategy, grid-independent study, calibration and test-

* Corresponding authors.
E-mail addresses: kaili_zhang@hotmail.com (K.L. Zhang), mpecsk@nus.edu.sg (S.K. Chou).
[1] Postal address: Micro/Nano Systems Initiative (MNSI), Department of Mechanical Engineering, National University of Singapore, Singapore 119260; Tel.: (65) 68742215; fax: (65) 67791459.

1290-0729/$ – see front matter
doi:10.1016/j.ijthermalsci.2006.08.002

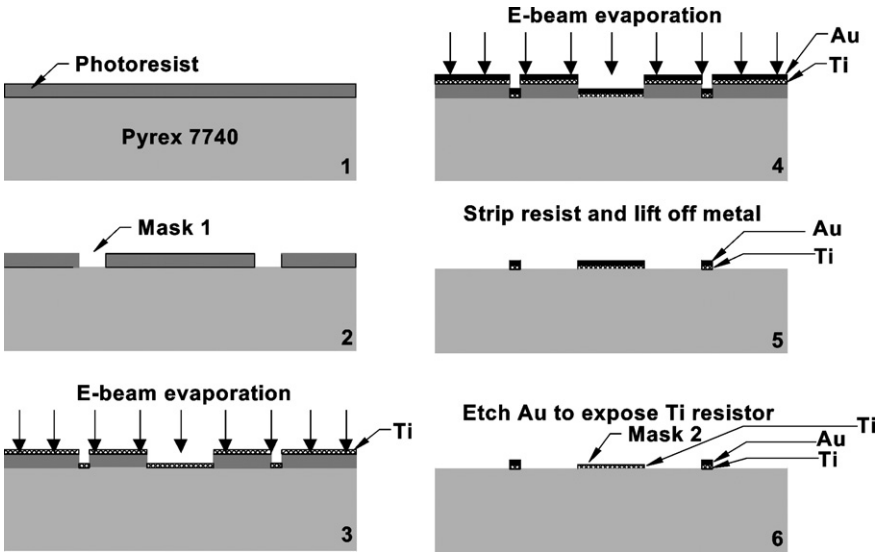

Fig. 1. Au/Ti microheater fabrication process flow.

ing procedures are sometimes missing. These are very useful for understanding the modeling and experiment accuracy.

In this paper, a thin film Au/Ti microheater deposited on a Pyrex-7740 glass substrate is developed. Pyrex-7740 glass is selected as the bulk substrate of the microheater because of its lower thermal conductivity and higher electrical resistivity compared to silicon, thus achieving good heat confinement and low power consumption. The Ti layer acts as both the resistor and the adhesion layer between Au and glass. The Au layer acts as both the conductor and the contact pad. The fabrication process is much easier and fabrication yield is much higher than the realization of dielectric membrane-based microheaters [3–5,8]. This kind of microheater is especially useful for short temperature pulse applications, like microthruster ignition and micro explosive boiling. Being based on a bulk Pyrex substrate, it is furthermore compatible with harsh environments, which is generally not the case for membrane-based microheaters. A finite-element based electro-thermal modeling is presented to predict the microheater performance. The electrical resistivity and thermal conductivity of thin film Au/Ti are crucial to the modeling and they are very much different from those of bulk Au/Ti due to differences in their microstructures. No existing electrical resistivity and thermal conductivity data of thin film Au/Ti could be found in the literature. Therefore, a method is presented to determine the thin film Au/Ti electrical resistivity and thermal conductivity. In addition, some interesting differences in heat transfer between a microheater and a conventional heater are addressed in the modeling. Furthermore, the Au/Ti microheater temperatures from the modeling are compared with those obtained from experimental measurements.

2. Fabrication of the thin film Au/Ti microthruster

The fabrication was performed using a micro fabrication technology. The process started with a 550 μm thick double polished Pyrex 7740 glass substrate. Positive photoresist was spin-coated onto the Pyrex glass and patterned using photolithography through a designed mask-1. A metal layer of Ti with the thickness of 206 nm (measured with a Profiler from KLA-Tencor Corporation) was deposited on the glass substrate by e-beam evaporation. The Ti layer acts as both the resistor and the adhesion layer. Then a metal layer of Au with the thickness of 77 nm was deposited onto the Ti layer through e-beam evaporation. The Au layer acts as both the conductor and contact pad. Metal (Ti and Au) lift-off was performed in an ultrasonic bath using acetone for 20 min. After solvent and DI-water clean, the Pyrex substrate with Ti and Au metals was spin-coated and patterned using photolithography by another designed mask-2. After the exposed photoresist was removed, the substrate was put into Au etchant ($KI + I_2 + H_2O$) for 5 min. The Au in the designed area was removed and the zigzag Ti was exposed as the resistor. After solvent and DI-water clean, the glass wafer with the Au/Ti microheater was blown-dried with nitrogen and then put into an oven with nitrogen flux at 250 °C for 20 min. The simplified micro fabrication process is shown in Fig. 1.

Fig. 2 is the SEM photo of the fabricated microheaters with Ti as the resistor and Au as the conductor. The optical photo of

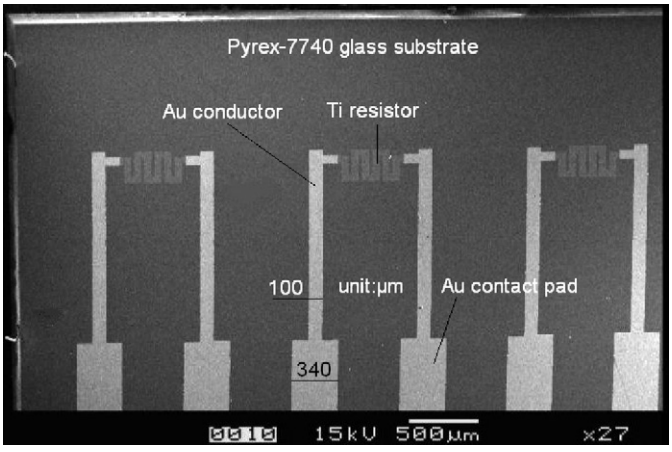

Fig. 2. SEM photo of the Au/Ti microheater.

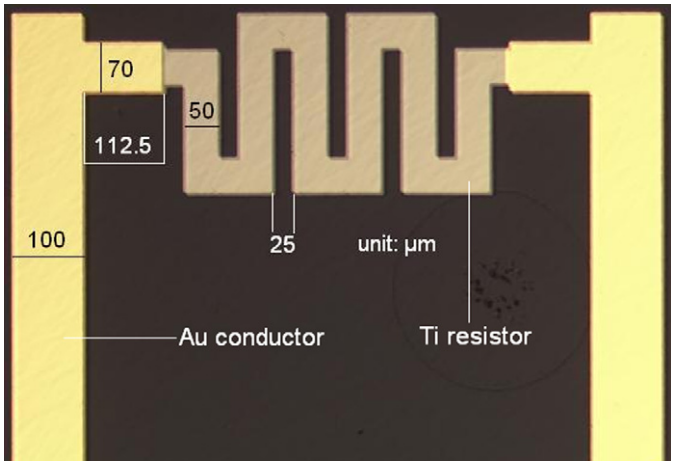

Fig. 3. Optical photo of the Au/Ti microheater.

the zigzag part of Ti resistor is shown in Fig. 3. The dimensions of the single microheater structure are about 3500 × 1500 × 550 μm (L × W × T) and the dimensions of the heater zone (hotspot) are 475 × 250 μm.

3. Three-dimensional finite-element electro-thermal modeling

3.1. Microheater geometry

The dimensions of the simulated Au/Ti microheater are exactly the same as the fabricated Au/Ti microheater (see Figs. 2 and 3). The geometry of the simulated Au/Ti microheater is shown in Fig. 4.

3.2. Material property

The electrical resistivity, thermal conductivity, total emissivity, specific heat, and density of the thin film Au, thin film Ti, and Pyrex-7740 glass are required in the modeling. The Au and Ti thin films are the key materials for the electro-thermal process. Their properties can be affected by the deposition and fabrication conditions. Consequently, the properties of these thin film materials must be determined carefully.

3.2.1. Electrical resistivity of thin film gold

The electrical resistivity of Au can be found in Ref. [11]. Nevertheless, the data for bulk Au cannot be used for thin film Au due to the differences in their microstructures. Employing Matthiessen's Rule [12], the thin film Au resistivity is estimated by combining the measured thin film Au resistivity at room temperature (300 K) with the temperature-variation data from Ref. [11]. According to Matthiessen's Rule, the resistivity of a metal is composed of two components. One is the "residual" resistivity ρ_0, which is independent of temperature. The other is the lattice resistivity $\rho_l(T)$, due to the vibrating lattice. The two resistivities can be separated and $\rho_l(T)$ would be the same for the bulk and thin film metals. As a result,

$$\rho_{\text{bulk/thin-film}}(T) = \rho_{0,\text{bulk/thin-film}} + \rho_l(T) \tag{1}$$

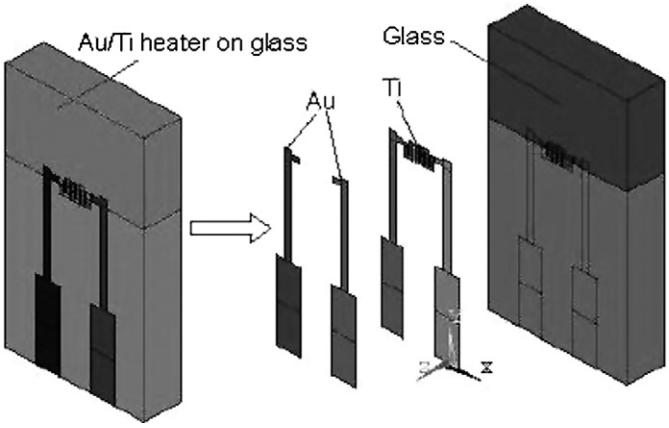

Fig. 4. Geometry of the simulated Au/Ti microheater.

Therefore, the difference between thin film Au resistivity and bulk Au resistivity is

$$\begin{aligned}\Delta\rho &= \rho_{\text{thin-film}}(T) - \rho_{\text{bulk}}(T) = \rho_{0,\text{thin-film}} - \rho_{0,\text{bulk}} \\ &= \rho_{\text{thin-film}}(300\ \text{K}) - \rho_{\text{bulk}}(300\ \text{K})\end{aligned} \tag{2}$$

Accordingly, the data of bulk Au resistivity in Ref. [11] can be modified for the thin film Au by adding $\Delta\rho$

$$\rho_{\text{thin-film}}(T) = \rho_{\text{bulk}}(T) + \Delta\rho \tag{3}$$

The thin film Au resistivity at room temperature ($\rho_{\text{thin-film}}(300\ \text{K})$) is measured by a Veeco FPP-5000 4-Point Probe. An Au layer with a thickness of 77 nm is deposited by e-beam onto a silicon wafer covered with a SiO_2 insulation layer. The deposition conditions are the same as those employed for the Au/Ti microheater fabrication. The sheet resistivity of Au at 300 K is measured using the 4-Point Probe. The resistivity of Au is obtained through multiplying the sheet resistivity by 77 nm. The measured resistivity of thin film Au at 300 K is 3.99×10^{-8} Ω·m, which is higher than the bulk Au resistivity of 2.77×10^{-8} Ω·m in Ref. [11]. This higher resistivity is caused by the low deposition temperature, not allowing for diffusion of individual Au atoms during the deposition to form a lattice of a lower defect density as compared to the bulk Au. Table 1 is the estimated thin film Au resistivity using Eq. (3).

3.2.2. Thermal conductivity of thin film gold

The thermal conductivity of bulk Au can be found in Ref. [11]. The data must be modified for thin film Au due to the different microstructures. For metallic Au, the relationship of its thermal conductivity κ and electrical conductivity σ ($\sigma = 1/\rho$) is described by Wiedemann–Franz Law [12]:

$$\frac{\kappa}{\sigma} = \kappa\rho = LT \tag{4}$$

where L, called the Lorentz number, is 2.41×10^{-8} W·Ω/K^2 for Au [11,12]. Wiedemann–Franz Law is used to obtain the thin film Au thermal conductivity at 300 K with a value of 180.93 W/m K. The inverse of the Au thermal conductivity ($1/\kappa$, called thermal resistivity) is assumed to have two components. One is caused by lattice defects ($1/\kappa_0$) and the other

Table 1
Estimated electrical resistivity of thin film Au

Temperature (K)	293	298	300	400	500	600	700	800	900
Resistivity (10^{-8} Ω·m)	3.94	3.98	3.99	4.83	5.69	6.6	7.55	8.54	9.59

Table 2
Estimated thermal conductivity of thin film Au

Temperature (K)	293	300	400	500	600	800
Conductivity (W/mK)	181.1	180.93	178.96	176.62	174.58	169.68

Table 3
Estimated electrical resistivity of thin film Ti

Temperature (K)	293	300	400	500	600	700	800	900
Resistivity (10^{-8} Ω·m)	153.55	156.35	175.35	194.55	214.05	231.15	245.75	257.35

Table 4
Estimated thermal conductivity of thin film Ti

Temperature (K)	293	300	400	500	600	700	800
Conductivity (W/m K)	5.94	5.93	5.81	5.76	5.72	5.73	5.76

is due to thermal vibrations ($1/\kappa_l(T)$) in analogy to electrical resistivity.

$$\frac{1}{\kappa(T)} = \frac{1}{\kappa_0} + \frac{1}{\kappa_l(T)} \tag{5}$$

The thermal resistivity difference $\Delta(1/\kappa)$ between thin film and bulk Au is expressed as

$$\Delta\left(\frac{1}{\kappa}\right) = \frac{1}{\kappa_{\text{thin-film}}(T)} - \frac{1}{\kappa_{\text{bulk}}(T)} = \frac{1}{\kappa_{0,\text{thin-film}}} - \frac{1}{\kappa_{0,\text{bulk}}} = \frac{1}{\kappa_{\text{thin-film}}(300\ \text{K})} - \frac{1}{\kappa_{\text{bulk}}(300\ \text{K})} \tag{6}$$

Consequently,

$$\kappa_{\text{thin-film}}(T) = \left(\frac{1}{\kappa_{\text{bulk}}(T)} + \Delta\left(\frac{1}{\kappa}\right)\right)^{-1} \tag{7}$$

The thermal conductivity of thin film Au is estimated by Eq. (7) and listed in Table 2.

3.2.3. Electrical resistivity and thermal conductivity of thin film titanium

The electrical resistivity and thermal conductivity of thin film Ti are obtained in a similar manner as those of thin film Au. The thin film Ti electrical resistivity at 300 K is measured by a 4-point probe. The thin film Ti resistivity as a function of temperature is calculated using the Matthiessen's rule and bulk Ti resistivity data [11]. On the other hand, the thermal conductivity of thin film Ti is obtained from the Wiedemann–Franz Law and bulk Ti thermal conductivity data [11]. Tables 3 and 4 are the estimated data for thin film Ti.

3.2.4. Total emissivity and specific heat of thin film titanium and gold

The total emissivityε of titanium has been studied in Ref. [13]. These values assume a smooth surface. Because titanium is deposited onto a very smooth glass surface in this work, it is indeed smooth and the emissivity values from Ref. [13] do not need to be modified as listed in Table 5.

The total emissivity of Au is obtained from Ref. [14] with 0.02 at 473 K and 0.03 at 873 K.

The specific heats for the thin film Ti and Au are assumed to be similar to those of the bulk Ti and Au [11] as listed in Table 6.

3.2.5. Summary of material properties

Table 7 shows the summary of the properties of the materials used in the modeling. The properties of bulk Pyrex-7740 glass are from its supplier.

3.3. Initial condition and boundary conditions

For this transient modeling, the initial temperature of the entire microheater is assumed to be 300 K. The boundary conditions are as follows: the ambient temperature is 300 K, heat convection and radiation on all the surfaces of the microheater in contact with ambient air, and ohmic heating in the element volumes.

4. Modeling results

For this transient electro-thermal process, finite-element modeling software ANSYS is used here to model the entire three-dimensional device due to its excellent capacity to solve multi-physics problems in microscale [4,8,15]. For efficient and accurate modeling, appropriate meshing for the microheater should be determined. The thin film Au/Ti has the finest mesh to model the electro-thermal process more accurately as shown in

Table 5
Estimated total emissivity of thin film Ti

Temperature (K)	366	478	589	700	811	922	1033	1144	1255
Total emissivity	0.3	0.3	0.3	0.3	0.31	0.31	0.32	0.35	0.41

Table 6
Estimated specific heats for the thin film Ti and Au

Temperature (K)	300	350	400	500	600
Specific heat (Ti, J/kg K)	129	129	130	133	136
Specific heat (Au, J/kg K)	0.3	0.3	0.3	0.3	0.31

Table 7
Summary of material properties

	Pyrex-7740	Thin film Au	Thin film Ti
Electrical resistivity (Ω·m)	1.26×10^6	$\rho(T)$	$\rho(T)$
Thermal conductivity (W/m K)	1.18	$\kappa(T)$	$\kappa(T)$
Specific heat (J/kg K)	753.12	$Cp(T)$	$Cp(T)$
Total emissivity		$\varepsilon(T)$	$\varepsilon(T)$
Density (kg/m^3)	2230	19320	4507

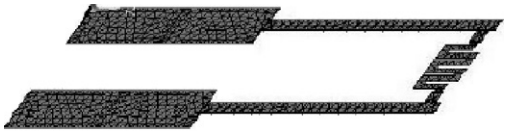

Fig. 5. Meshed thin film Au/Ti layers.

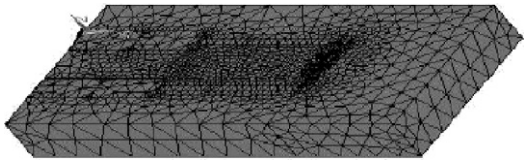

Fig. 6. Meshed glass layer.

Fig. 5. For the glass substrate, the region near Au/Ti is meshed finely to match the Au/Ti mesh and to capture the conductive heat transfer; the mesh becomes coarser away from this region as shown in Fig. 6.

The computational grids employed for the modeling are determined by performing grid-independent study to minimize the modeling error. When the change in the solution between subsequent stages of grid refinement is considered to be negligible, the lower, but still sufficient, grid resolution is kept. The Au/Ti microheater maximum temperature is compared among different stages of grid refinement as shown in Fig. 7. Finally, the model is meshed using 38320 nodes.

4.1. Initial comparison between experiment and modeling

A simple experiment is performed to visually verify the finite-element model. An Au/Ti microheater is connected to a high voltage power source for a long time so that part of the Ti is damaged because of long exposure to high temperature. A photo is taken at the Ti part of the Au/Ti microheater using a microscope as shown in Fig. 8. As can be seen, the discolored portions of the Ti heater are caused by excessive heat generation. The simulated temperature profile of the Ti heater from finite-element modeling is shown in Fig. 9. As is shown, both the temperature profiles from the experiment and modeling match very well. A more precise temperature comparison between experiment and modeling is presented next.

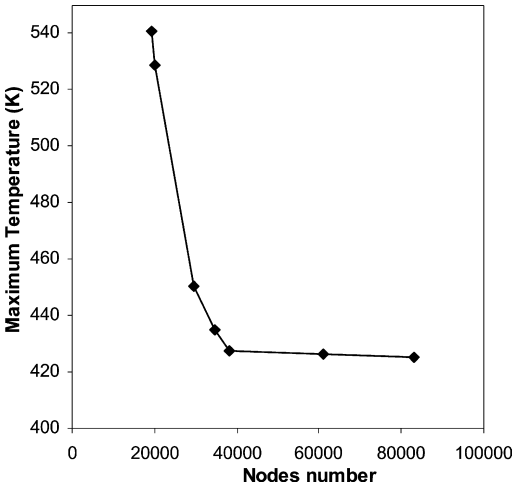

Fig. 7. Grid-independent study.

Fig. 8. Temperature profile from experiment.

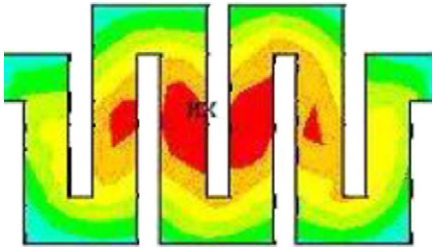

Fig. 9. Temperature profile from modeling.

4.2. Effect of heat convection on microheater maximum temperature

For a conventional heater, convection heat loss is normally a crucial factor that affects the heater performance. However, for micro-scale heater, this may not be the case. To study the effect of heat convection on microheater performance, modeling is performed for the thin film Au/Ti microheater using convection coefficient values range from 10 to 100 W/m^2 K. Fig. 10 shows the microheater maximum temperatures with an 8 V supply voltage at different convection coefficients. When the microheater maximum temperature is lower than 660 K, the

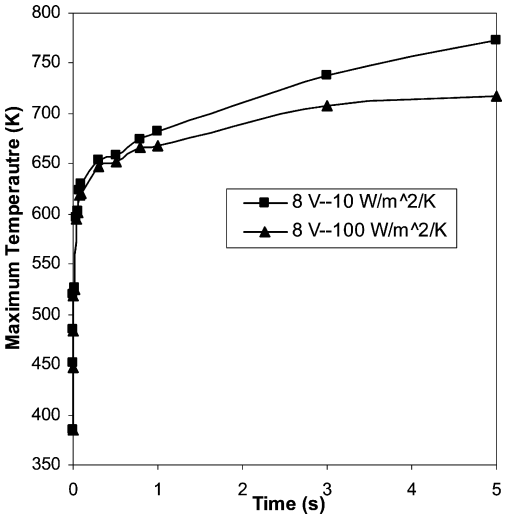

Fig. 10. Effect of heat convection on microheater temperature.

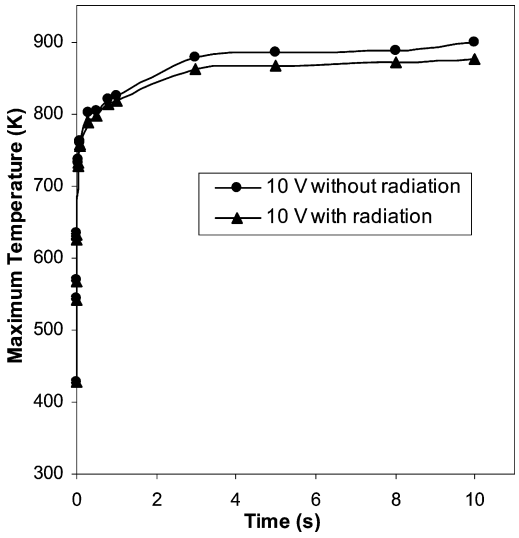

Fig. 11. Effect of radiation on microheater temperature.

temperature difference is below 1% even if the convection coefficient changes from 10 to 100 W/m^2 K. When the maximum temperature is below 800 K, the difference is within 10%. Because the microheater normal operation maximum temperature is below 800 K, the impact of heat convection on the Au/Ti microheater temperature can then be neglected. Therefore, the heat convection is supposed to be negligible at median-low temperatures because of the small size of the microheater. This is wastly different from that for a conventional heater. Puigcorbe et al. also validated this phenomenon for polysilicon a microheater deposited on a silicon substrate with dielectric membranes [4]. Rossi et al. estimated the heat convection coefficient to be 100 W/m^2 K using infra-red (IR) method for their polysilicon microheater [8]. The device dimensions and conditions in Ref. [8] are similar to those of the microheater in this study. Hence, 100 W/m^2 K is employed for the following simulations.

4.3. Thermal radiation effect on microheater maximum temperature

Thermal radiation is another important way of heat loss, especially for high temperature objects. Because the microheater is supposed to operate in the high temperature range, the radiation heat loss of the microheater should be addressed. Fig. 11 shows the effect of radiation heat loss on the microheater maximum temperature with a 10 V supply voltage. The microheater maximum temperature changes only 2.43% because of radiation loss even if the microheater maximum temperature increases to 898.74 K. Consequently, the radiation heat loss is neglected in the following simulations.

4.4. Microheater temperature variation with time and space

The microheater temperature variation with time and space is very useful for understanding the thin film heater performance. Figs. 12 to 15 show the microheater temperature (K) variation from 1 ms to 10 s with a 10 V supply voltage. For a thin film heater, minimizing thermal heat loss is the key to gain

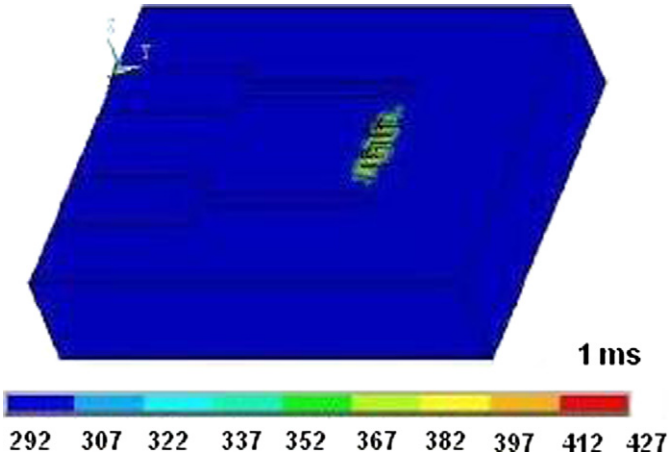

Fig. 12. Temperature profile at 1 ms.

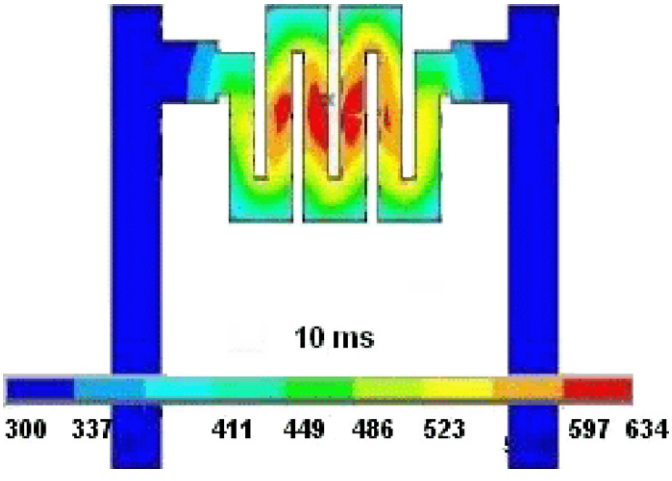

Fig. 13. Ti resistor temperature profile at 10 ms.

a better thermal yield (maximum temperature over the electrical power consumption). One way to reduce considerably thermal loss is to have a very good heat confinement. It can be seen from these figures that a good heat confinement is achieved for the

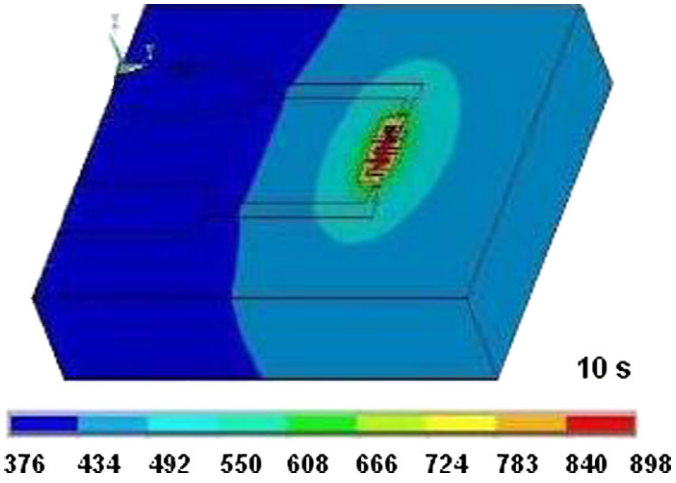

Fig. 14. Temperature profile at 10 s.

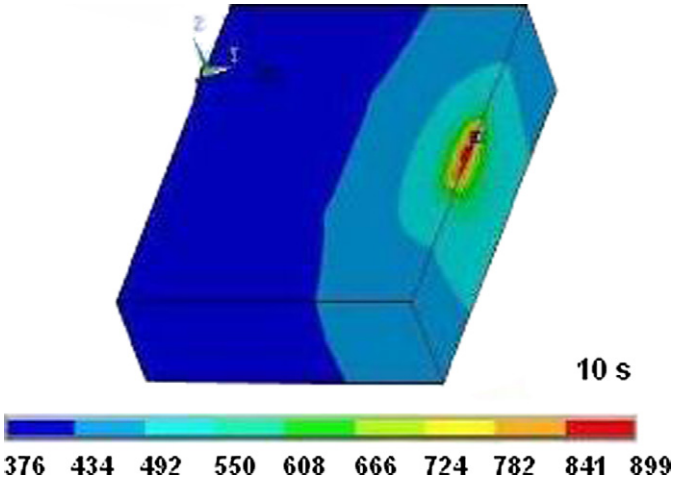

Fig. 15. Temperature profile at 10 s.

Au/Ti microheater. The temperature at the Ti heater increases rapidly, whereas the temperature does not change very much elsewhere. This is mainly caused by the zigzag microheater design and the better thermal insulation property of Pyrex 7740 glass substrate compared to silicon substrate (thermal conductivity: Pyrex 7740 glass, 1.18 W/m K; silicon, 141.2 W/m K). The cross-section view of the substrate temperature profile is shown in Fig. 15.

4.5. Microheater maximum temperature variation with voltage

The maximum temperature is a key parameter of the microheater, especially for micro ignition application [9,10]. Fig. 16 shows the microheater maximum temperature variation as a function of the supply voltage. The variation in temperature follows a logarithmic trend. The plots indicate that the maximum temperature increases rapidly at the application of the power, but the increase is slow after about 4 s. This is due to the equilibrium between heat generation by the Joule effect and heat loss by conduction, convection and radiation. As can be seen, the microheater maximum temperature can be controlled by changing the supply voltage.

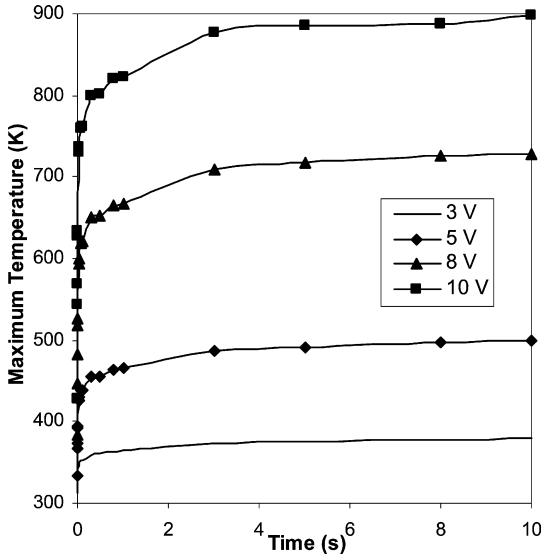

Fig. 16. Microheater maximum temperature variation with voltage.

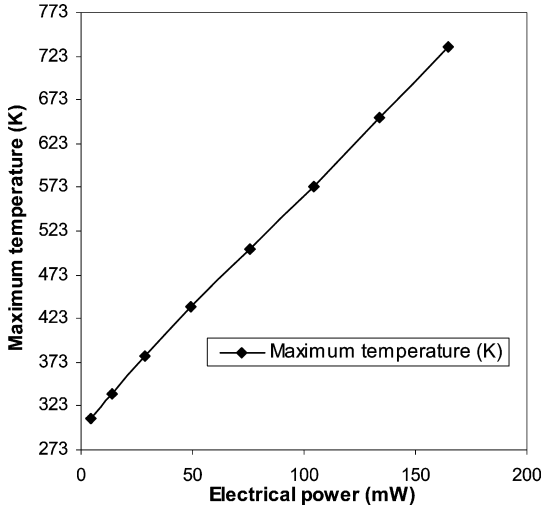

Fig. 17. Microheater maximum temperature versus electrical power.

4.6. Microheater maximum temperature versus electrical power

One of the main requirements for a thin film microheater is low power consumption. Fig. 17 shows the microheater maximum temperature variation as a function of the electrical power at steady state. As is shown, the variation in maximum temperature follows a linear trend with electrical power, which is similar to that for polysilicon heater developed in Ref. [8]. The microheater has a good thermal yield (437 K at an input power of 50 mW, 573 K at 100 mW). This is due to the zigzag heater geometry and high thermal resistance of the Pyrex 7740 glass compared to silicon.

5. Experimental testing of the thin film Au/Ti microheater

A custom-circuitry was fabricated to measure the transient temperature of the Au/Ti microheater experimentally [16]. In this set-up, the microheater temperature is determined indi-

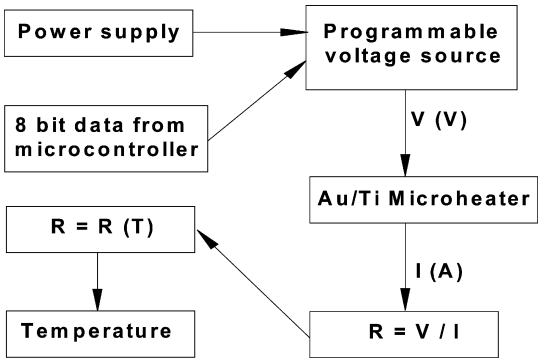

Fig. 18. Principle of acquiring the microheater temperature.

rectly by measuring the change in electrical resistance of the microheater. This method has been shown to be an accurate method for obtaining the transient temperature of micro-scale heaters [6,7]. In this measurement, an experimental calibration law of the microheater electrical resistance versus temperature is used to infer the actual temperature of the microheater. Fig. 18 shows the principle of acquiring the microheater temperature. The change in the microheater resistance is first calculated using Ohm's law ($R = V/I$). Then, the transient temperature of the microheater is obtained using the formula derived from the calibration law.

5.1. Calibration of the microheater resistance versus temperature

A silicon chip with a SiO_2 insulation layer and Au contact pads was employed to hold the microheater. The Au contact pads of the microheater were connected to Au contact pads on the SiO_2 layer by a thin Au wire using ultrasonic bonding. Two flexible wires were connected to the Au contact pads on the SiO_2 layer using a high-temperature solder. Then, the microheater installed on the silicon chip was placed into a Carbolite 1200 burn-off furnace. The furnace temperature and the microheater electrical resistance were measured simultaneously using an HP 34970A data acquisition unit. The furnace temperature was increased slowly to allow for thermal equilibrium and measured by taking the average readings of two type-K thermocouples mounted very close to the microheater. The microheater resistance was measured using a four-wire technique to improve the measurement accuracy. From the measurement data, a calibration law, $R = 0.3522T + 249.13$, is derived.

5.2. Microheater temperature variation with time

Fig. 19 shows the changes in supply current as a function of time at an 8 V supply voltage for the Au/Ti microheater along with its corresponding change in microheater resistance.

From these data, the temperature variation of the microheater with an 8 V supply can be deduced from the calibration law and is shown in Fig. 20. The average temperature increases very quickly at the application of the supply voltage but the increase is slow after 4 s. Again, this is due to the equilibrium

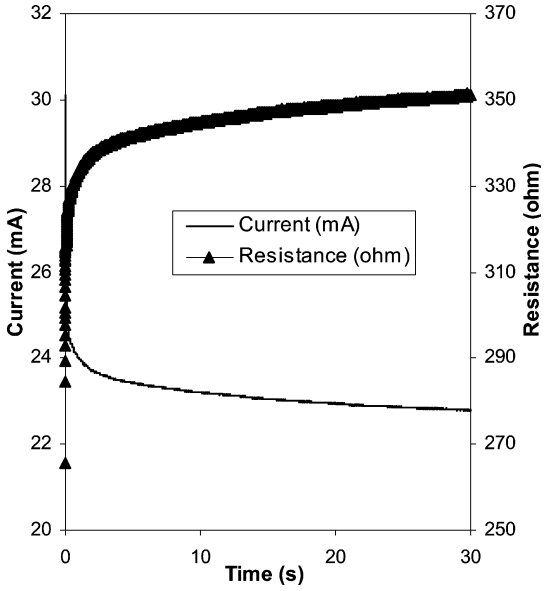

Fig. 19. Current and resistance variations with time.

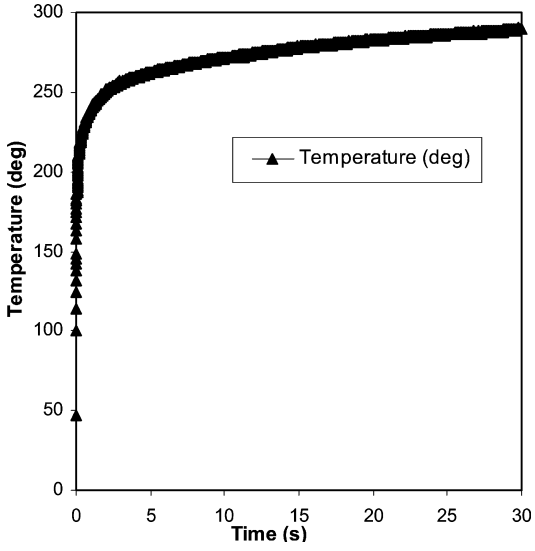

Fig. 20. Au/Ti microheater temperature variation with time.

between heat generation by the Joule effect and heat loss by conduction, convection, and radiation.

5.3. Comparison between experimental measurement and electro-thermal modeling

Fig. 21 shows the distribution of electric field in the Au/Ti microheater with a supply voltage of 8 V from electro-thermal modeling. As can be seen, almost all the voltage drop occurs in the zigzag part of the Ti resistor, which is expected because thin film Au has a much lower electrical resistivity than that of thin film Ti. This means the Au contact pad and Au conductor resistance can be neglected. Therefore, the calibration law of resistance versus temperature of the microheater corresponds to that on the zigzag part of the Ti microheater. Consequently, the average temperature of the Ti zigzag part can be derived from

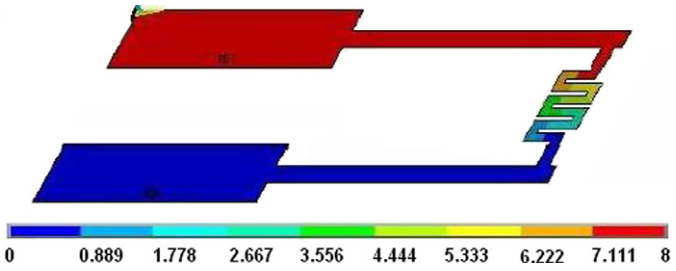

Fig. 21. Electrical field of the Au/Ti microheater.

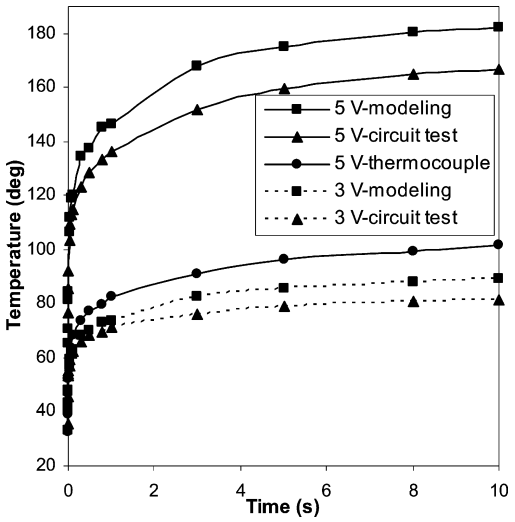

Fig. 22. Comparison between measurements and electro-thermal modeling.

electro-thermal modeling for comparison with the experimental measurements.

Fig. 22 shows the microheater temperature comparison among electro-thermal modeling, experimental measurements using the circuitry and a type-K thermocouple at supply voltages of 3 and 5 V. The thermocouple was attached tightly to zigzag part of the microheater. Temperature was acquired using an Agilent 34970A data acquisition unit with a scan rate of 1 ms. As can be seen, temperatures obtained from the type-K thermocouple are much lower than those from both the modeling and custom-circuitry measurements. This is mainly caused by thermocouple heat conduction as well as the presence of a thermal resistance between the thermocouple and microheater. This shows that direct thermocouple measurement is not very practical for micro-scale heater. The temperature difference between electro-thermal modeling and experimental measurement using the custom-circuitry is small. This difference is mainly caused by the variation between actual thin film Au/Ti material characteristics and those calculated in the modeling, the uncertainty in resistance versus temperature calibration, and the oxidation of Ti and degradation of Au/Ti due to agglomeration at high temperatures [17].

6. Conclusion

A thin film Au/Ti microheater deposited onto a Pyrex glass substrate was designed, fabricated, simulated and tested. The use of Pyrex glass reduced the microheater power consumption due to its lower thermal conductivity and higher electrical resistivity compared to silicon. The fabrication process of this Au/Ti microheater is simpler and has a higher yield than those of the microheaters employing dielectric membranes. A method was presented to investigate the thin film Au/Ti properties. The three-dimensional thin film microheater performance was predicted using a FEA-based electro-thermal modeling. It was found that heat conduction through the substrate dominated the microheater heat loss, whereas, heat convection and heat radiation losses were negligible at median-low temperatures due to the small size of the microheater. The transient temperature response with the application of power supply was determined by measuring the change in resistance versus time using a fast custom data acquisition circuitry. Experimental measurements were found to validate the electro-thermal modeling.

References

[1] M.A. Gajda, H. Ahmed, Applications of thermal silicon sensors on membranes, Sensors and Actuators A 49 (1–2) (1995) 1–9.
[2] S.K.H. Fung, Z. Tang, P.C.H. Chan, J.K.O. Sin, P.W. Cheung, Thermal analysis and design of a micro-hotplate for integrated gas-sensor applications, Sensors and Actuators A 54 (1–3) (1996) 482–487.
[3] D. Briand, A. Krauss, B. van der Schoot, U. Weimar, N. Barsan, W. Göpel, N.F. de Rooij, Design and fabrication of high-temperature micro-hotplates for drop-coated gas sensors, Sensors and Actuators B 68 (1–3) (2000) 223–233.
[4] J. Puigcorbe, D. Vogel, B. Michel, A. Vila, I. Gracia, C. Cane, J.R. Morante, Thermal and mechanical analysis of micromachined gas sensors, Journal of Micromechanics and Microengineering 13 (5) (2003) 548–556.
[5] M. Baroncini, P. Placidi, G.C. Cardinali, A. Scorzoni, Thermal characterization of a microheater for micromachined gas sensors, Sensors and Actuators A 115 (1) (2004) 8–14.
[6] Y. Iida, K. Okuyama, Boiling nucleation on a very small film heater subjected to extremely rapid heating, International Journal of Heat and Mass Transfer 37 (17) (1994) 2771–2780.
[7] S. Glod, D. Poulikakos, Z. Zhao, G. Yadigaroglu, An investigation of microscale explosive vaporization of water on an ultra thin Pt wire, International Journal of Heat and Mass Transfer 45 (2) (2002) 367–379.
[8] C. Rossi, E. Scheid, D. Esteve, Theoretical and experimental study of silicon micromachined microheater with dielectric stacked membranes, Sensors and Actuators A 63 (3) (1997) 183–189.
[9] D.H. Lewis Jr., S.W. Janson, R.B. Cohen, E.K. Antonsson, Digital Micropropulsion, Sensors and Actuators A 80 (2) (2000) 143–154.
[10] K.L. Zhang, S.K. Chou, S.S. Ang, X.S. Tang, A MEMS-based solid propellant microthruster with Au/Ti microheater, Sensors and Actuators A 122 (1) (2005) 113–123.
[11] D.R. Lide (Ed.), CRC Handbook of Chemistry and Physics, 79th ed., CRC Press, Boca Raton, 1998–1999.
[12] C. Kittel, Introduction to Solid State Physics, seventh ed., John Wiley and Sons, New York/Singapore, 1996, pp. 159–162, 166–168.
[13] W.D. Wood, H.W. Deem, C.F. Lucks, in: The Emittance of Titanium and Titanium Alloys, Defense Metals Information Center, Battelle Memorial Institute, Columbus, OH, 1969, p. 4.
[14] R.C. Weast (Ed.), CRC Handbook of Chemistry and Physics, CRC Press, Boca Raton, FL, 1984–1985, p. E-380.
[15] ANSYS Reference Manual, ANSYS, Inc., PA, http://www.ansys.com/.
[16] K.L. Zhang, S.K. Chou, S.S. Ang, A wireless addressing circuitry for microthruster array, PowerMEMS 2005, Tokyo, Japan, November 28–30, 2005, pp. 105–108.
[17] S.L. Firebaugh, K.F. Jensen, M.A. Schmidt, Investigation of high temperature degradation of platinum thin films with an in-situ resistance measurement apparatus, Journal of Microelectromechanical Systems 7 (1) (1998) 128–135.